Journal of Alloys and Compounds 509 (2011) 8590–8594

Contents lists available at ScienceDirect

Journal of Alloys and Compounds

journal homepage: www.elsevier.com/locate/jallcom

Effect of Bi^{3+} doping on the quenching concentration of $^2H_{11/2}/^4S_{3/2}$ level of Er^{3+}

Mingzhu Yang[a,b,*], Yu Sui[b,c], Shuchen Lü[d], Mingji Wang[a], Xianjie Wang[b], Muhong Wu[b], Yang Wang[b], Tianquan Lü[b], Wanfa Liu[e]

[a] College of Electronic Science, Northeast Petroleum University, Daqing 163000, People's Republic of China
[b] Center for Condensed Matter Science and Technology (CCMST), Department of Physics, Harbin Institute of Technology, Harbin 150001, People's Republic of China
[c] International Center for Materials Physics, Academia Sinica, Shenyang 110015, People's Republic of China
[d] Department of Physics, Harbin Normal University, Harbin 150001, People's Republic of China
[e] Dalian Institute of Chemical Physics, Dalian 116023, People's Republic of China

HIGHLIGHTS

- The quenching concentration of $^2H_{11/2}/^4S_{3/2}$ levels of Er^{3+} increases by 2 mol% after the doping of 1.5 mol% Bi^{3+}.
- The green emission is enhanced 1.9 times by the doping of Bi^{3+}.
- The enhancement of green emission comes from the increases in both quenching concentration of $^2H_{11/2}/^4S_{3/2}$ and radiative transition.

ARTICLE INFO

Article history:
Received 20 December 2010
Received in revised form 8 June 2011
Accepted 13 June 2011
Available online 7 July 2011

Keywords:
Luminescence
Optical materials
Optical properties
Sol–gel process

ABSTRACT

Bi^{3+} and Er^{3+} codoped Y_2O_3 was prepared by sol–gel method. The upconversion emission was investigated under 980 nm excitation. For samples without Bi^{3+}, the quenching concentration of $^2H_{11/2}/^4S_{3/2}$ level of Er^{3+} is 3.0 mol%. However, by 1.5 mol% Bi^{3+} doping the quenching concentration increases to 5.0 mol%; meanwhile, the green emission is enhanced 1.9 times. The results indicate that both the quenching concentration and the emission intensity of $^2H_{11/2}/^4S_{3/2}$ level can be increased by Bi^{3+} doping.

1. Introduction

Rare-earth ions doped upconversion materials have recently attracted considerable attention for their applications in solid state visible lasers, color displays and biomedical imaging [1–3]. Among luminescent rare-earth ions, the Er^{3+} has, in recent years, attracted the most interest, mainly because its rich energy levels favor many upconversion processes. Patra et al. reported the effect of the Er^{3+} concentration in ZrO_2 on the upconverted emission [4]. Sun et al. investigated the influence of Li^+ on the upconversion luminescence spectra in Er^{3+} and Li^+ codoped $BaTiO_3$ nanocrystals [5]. The effect of the surface modification on the upconversion of Er^{3+} in $NaYF_4$ nanocrystals was studied by Li et al. [6]. As for the host for luminescent materials, most attention has been paid to oxide ceramics and nanopowders recently [7,8]. Y_2O_3 shows promise due to its high melting point, high chemical stability and low phonon energy [9].

Since the emission of most upconversion materials does not have enough intensity, increasing the upconversion efficiency of these materials is still a formidable challenge. It is known that concentration quenching originates from the interaction between neighboring ions. By increasing the doping concentration, the emission intensity of certain energy levels of rare earth ions increases below quenching concentration [10,11]. Furthermore, the intra-4f electronic transitions of rare earth ions are parity forbidden according to the quantum mechanical selection rules. However, the forbiddance can be partially broken when the rare earth ions situate at low symmetry sites [12,13]. Therefore, if we can enhance the quenching concentration of rare earth ions and break the symmetry around them at the same time, the emission intensity can be improved. Dou et al. have reported that the proper doping of lager-radius La^{3+} ion can break up the cluster of Yb^{3+} ion [14]. Moreover, as the radius of the doping ion is different from that of the host, the crystal field symmetry of the host can be modified by doping [12,13]. The radius of Bi^{3+} (1.03 Å) is larger than that of Y^{3+}

* Corresponding author.
E-mail address: yangmingzhu0000@163.com (M. Yang).

0925-8388/$ – see front matter © 2011 Elsevier B.V. All rights reserved.
doi:10.1016/j.jallcom.2011.06.037

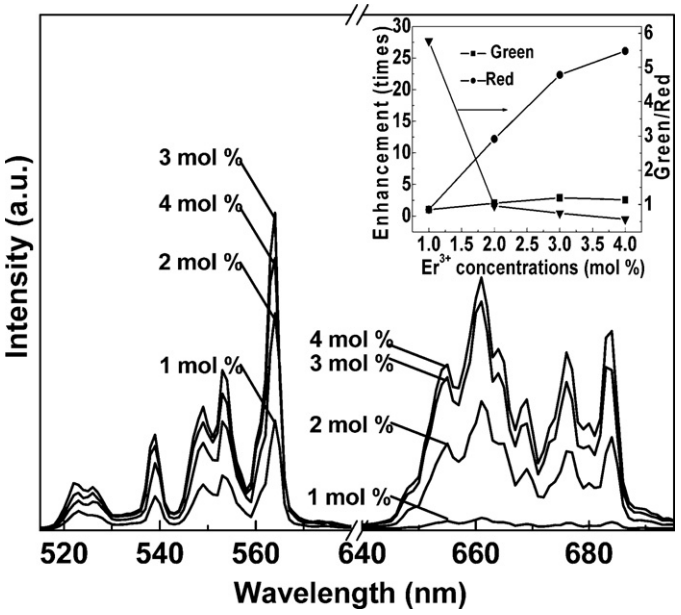

Fig. 1. Green and red upconversion emissions of Er^{3+}:Y_2O_3 powders with different concentrations of Er^{3+} under 980 nm excitation and an excitation power of 200 mW. The inset is the dependence of the intensity of the green and red upconversion emission as well as the ratio of Green/Red on the concentration of Er^{3+}.

(0.90 Å) [15], so with doping of Bi^{3+} the interaction of neighboring Er^{3+} ions could be weakened and the quenching concentration of Er^{3+} ion could be increased. Meanwhile the substitution of Bi^{3+} for Y^{3+} can modify the symmetry of the crystal field in the lattice and enhance the radiative transition rate, which favors the enhancement of upconversion emission intensity. In this study, the Er^{3+}/Bi^{3+}:Y_2O_3 powders were prepared and the influence of Bi^{3+} doping on the optical properties of Er^{3+}:Y_2O_3 was investigated.

2. Experimental

Y_2O_3 powders doped by Er^{3+} and Bi^{3+} with different concentrations were prepared by sol–gel combustion method. High-purity Y_2O_3 (99.99%), Er_2O_3 (99.99%), Bi_2O_3 (99.99%), and $C_6H_8O_7{\cdot}H_2O$ (Analytical reagent) were used as starting materials. Stoichiometric high-purity Y_2O_3, Er_2O_3 and Bi_2O_3 were dissolved in HNO_3 first. Then $C_6H_8O_7{\cdot}H_2O$ was added to the mixed solution with the molar ratio of nitrate to citric acid being 4:1. The resulting solution was heated to 80 °C in order to obtain a gel. Then the gel was rapidly heated to 200 °C and an autocombustion process took place. The precursor was calcined at 800 °C in air to obtain Er^{3+} and Bi^{3+} codoped Y_2O_3 powders. The upconversion emission spectra were measured by a power controllable 980 diode laser and detected with a lens-coupled monochromator with an attached photomultiplier. Decay profiles were measured by square-wave modulation of the electric current input to the 980 nm diode laser, and the signals were recorded by a Tektronix TDS 5052 digital oscilloscope with a lock-in preamplifier. The XRD data were recorded by a Rigaku D/max-γB diffractrometer using Cu K α radiation (λ = 0.15418 nm). The infrared absorption spectra were recorded with an IFS66V/S Fourier transform infrared spectrometer. The morphology of the samples was determined by the transmission electron microscope (TEM), JOEL 2010F.

3. Results and discussion

The upconversion emission spectra of different Er^{3+} concentrations in the Y_2O_3 upon 980 nm laser radiation are shown in Fig. 1, where two emission bands in the region of 515–640 and 640–695 nm are assigned to $^2H_{11/2}/^4S_{3/2} \rightarrow {}^4I_{15/2}$ and $^4F_{9/2} \rightarrow {}^4I_{15/2}$ transitions, respectively. The intensities of the two emission bands increase as the Er^{3+} concentration increases from 1.0 to 3.0 mol% and the decrease in the luminescence intensity of $^2H_{11/2}/^4S_{3/2} \rightarrow {}^4I_{15/2}$ transition occurs at the Er^{3+} concentration more than 3.0 mol%. However, the emission intensity of $^4F_{9/2} \rightarrow {}^4I_{15/2}$ transition still increases with increasing Er^{3+} content.

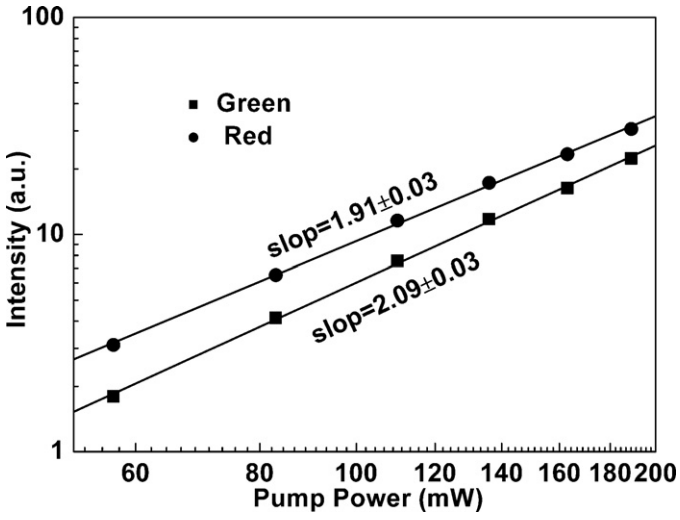

Fig. 2. The pump power dependence of the green and red upconversion emission intensity of 3 mol% Er^{3+}:Y_2O_3 powder.

To understand the mechanisms which populate the ($^2H_{11/2}/^4S_{3/2}$) green and ($^4F_{9/2}$) red emission levels, the upconversion luminescence intensity was measured as a function of the pump power. It is known that for unsaturated upconversion processes, the number of photons which are required to populate the upper emitting state can be obtained by the following relation [16]:

$$I \propto nP \quad (1)$$

where I is the intensity of emission, P is the laser pump power, and n is the number of photons needed to produce the emission. Fig. 2 shows that the slopes of the green and red emissions are both about 2, therefore, the upconversion occurs via a two-photon process. The upconversion processes of the green and red emissions can thus be described as Fig. 3. The Er^{3+} ion can be promoted to the $^4I_{11/2}$ state through the ground state absorption (GSA) process, and then nonradiative relaxation occurred and populated the $^4I_{13/2}$ state. Subsequently, $^4I_{11/2}$ and $^4I_{13/2}$ states are further excited to the $^4F_{7/2}$ and $^4F_{9/2}$ states respectively via excited state absorption (ESA) or energy transfer upconversion (ETU) processes. After that nonradiative relaxation processes populate the $^2H_{11/2}/^4S_{3/2}$ and $^4F_{9/2}$

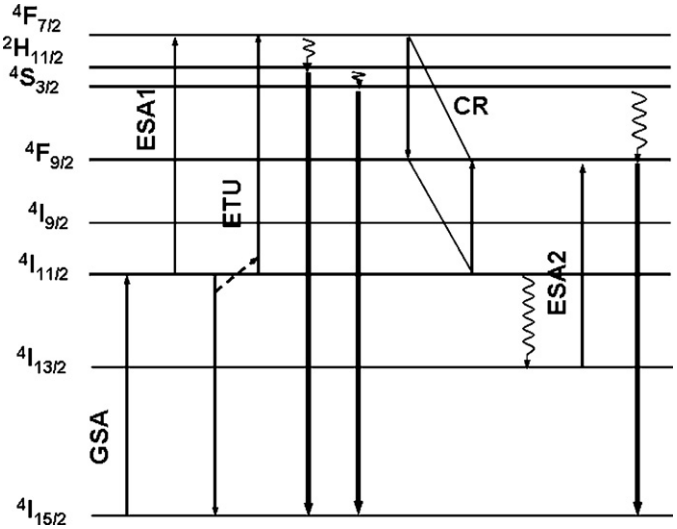

Fig. 3. Energy level diagram of Er^{3+} ion as well as the upconversion processes in Er^{3+}:Y_2O_3 powder under 980 nm excitation.

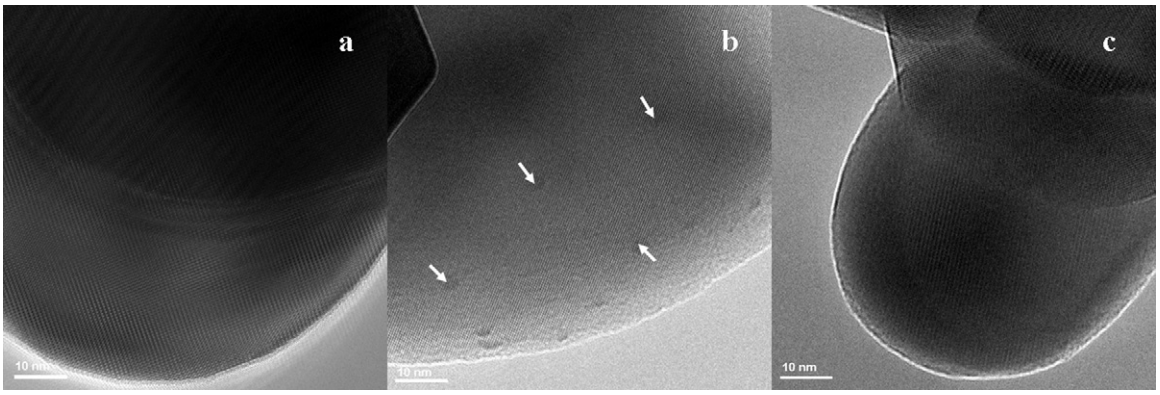

Fig. 4. TEM images of (a) 3 mol% Er^{3+}:Y_2O_3, (b) 4 mol% Er^{3+}:Y_2O_3, (c) 1.5 mol% Bi^{3+}/4 mol% Er^{3+}:Y_2O_3.

states. So the green and red emissions are observed by the transitions of $^2H_{11/2}/^4S_{3/2} \rightarrow {}^4I_{15/2}$ and $^4F_{9/2} \rightarrow {}^4I_{15/2}$. We consider that a cross-relaxation process is responsible for populating the $^4F_{9/2}$ level and occurs via two resonant transitions (Fig. 3): $^4F_{7/2} \rightarrow {}^4F_{9/2}$ and $^4F_{9/2} \leftarrow {}^4I_{11/2}$ [17]. The efficiency of the cross-relaxation process would increase with the decrease of the distance between the Er^{3+} ions. Therefore, the increasing Er^{3+} concentration gives rise to the enhancement of the red emission and the suppression of green emission (see Fig. 1). As shown in the inset of Fig. 1, the ratio of green to red emission decreases with increasing the Er^{3+} content.

The decrease of the distance between the Er^{3+} ions would lead to the formation of Er^{3+} clusters. Fig. 4 shows that there are no clusters in the sample doped with 3.0 mol% Er^{3+}, but some clusters are formed, indicated by arrows, in the sample doped with 4.0 mol% Er^{3+}. The cluster formation would effect the lifetime of the levels. As described in Fig. 5 the lifetime is measured to be 0.302 ms and 0.214 ms for the sample doped with 3.0 and 4.0 mol% Er^{3+}, respectively. This indicates that when the Er^{3+} clusters are formed the lifetime becomes shorter. It is known that the inverse of the lifetime is equal to the sum of the radiative transition and nonradiative relaxation rates [12]. When the Er^{3+} content increases to 4.0 mol% Er^{3+}, clusters are formed and the nonradiative cross-relaxation process increases. So the lifetime of $^4S_{3/2}$ level decreases obviously.

As mentioned above, the quenching of green emission originates from the cross-relaxation process with the increasing Er^{3+} concentration. In order to weaken the interaction between neighboring Er^{3+}, larger-radius Bi^{3+} is codoped in Er^{3+}:Y_2O_3. The XRD patterns

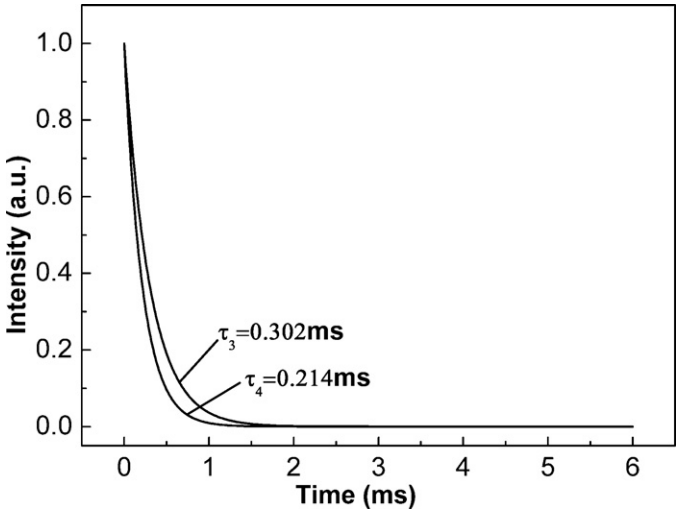

Fig. 5. The lifetime of $^4S_{3/2}$ level of Y_2O_3 powders doped with 3.0 and 4.0 mol% Er^{3+} under the excitation of 980 nm.

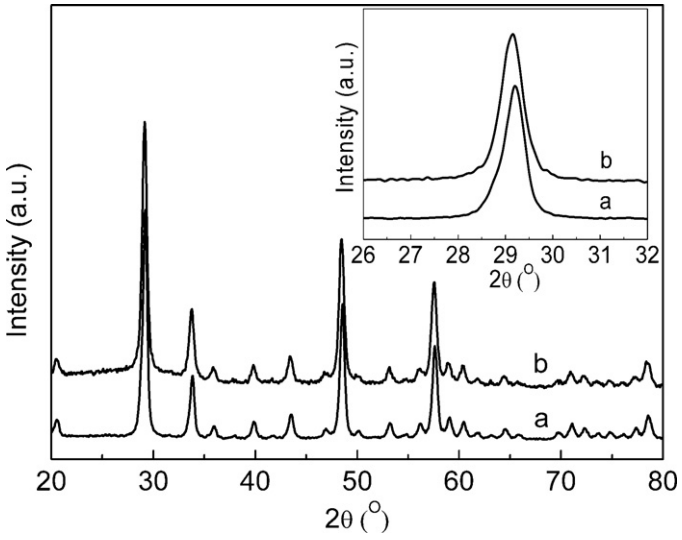

Fig. 6. XRD patterns of (a) 4 mol% Er^{3+}:Y_2O_3 and (b) 1.5 mol% Bi^{3+}/4 mol% Er^{3+}:Y_2O_3. The inset is the main diffraction peaks of the two samples.

of 4 mol% Er^{3+}:Y_2O_3 and 1.5 mol% Bi^{3+}/4 mol% Er^{3+}:Y_2O_3 are shown in Fig. 6. The XRD data confirms that both samples are single-phase with a cubic structure (JPDS No. 86-1107). However, the position of diffraction peaks shifts slightly with different doping concentrations. The inset of Fig. 6 shows the main diffraction peak of the two samples. It is clear that the main diffraction peak shifts toward smaller angles with Bi^{3+} doping. This indicates that the host lattice dimension expands after Bi^{3+} doping. The lattice parameters are listed in Table 1. The results show that Bi^{3+} and Er^{3+} were successfully doped into the Y_2O_3 host, and with the adding of Bi^{3+} the lattice parameter increases since the ion radius of Bi^{3+} is larger than that of Y^{3+}. The distance between Er^{3+} is thus increased after Bi^{3+} doping. The morphologies of Y_2O_3 doped with different concentrations of Er^{3+} and Bi^{3+} are shown in Fig. 4. It is clear that there are some clusters, indicated by arrows in 4 mol% Er^{3+}:Y_2O_3, but the clusters disappear after doping of Bi^{3+}. So the doping of larger-radius Bi^{3+} can enlarge the distance between neighboring Er^{3+} and dissociate the Er^{3+} clusters.

Table 1
The lattice parameters of Y_2O_3 doped with different contents of Er^{3+} and Bi^{3+}: (a) 4.0 mol% Er^{3+}:Y_2O_3 and (b) 1.5 mol% Bi^{3+}/4.0 mol% Er^{3+}:Y_2O_3.

Samples	a	b
Lattice parameter (Å)	10.5990	10.6091

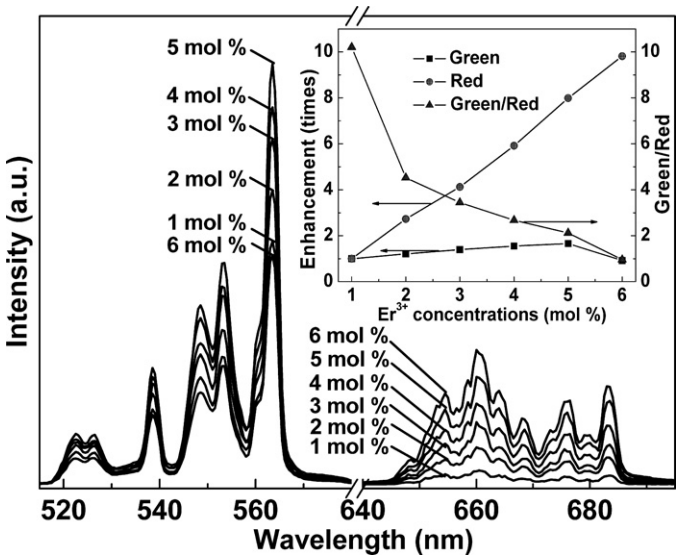

Fig. 7. Green and red upconversion emissions of $Bi^{3+}/Er^{3+}:Y_2O_3$ powders with different concentrations of Er^{3+} under 980 nm excitation and a excitation power of 200 mW. The inset is the dependence of the intensity of the green and red upconversion emission as well as the ratio of Green/Red on the concentration of Er^{3+}.

Fig. 7 shows the upconversion spectra of $Er^{3+}:Y_2O_3$ codoped with 1.5 mol% Bi^{3+}. As shown in Fig. 7, the quenching concentration of $^2H_{11/2}/^4S_{3/2} \rightarrow {}^4I_{15/2}$ transitions is 5.0 mol% which is increased by 2.0 mol% compared to the one without Bi^{3+}. As mentioned above, after Bi^{3+} doping, the distance between Er^{3+} ions is increased and the Er^{3+} clusters are dissociated. As a result, the interaction between neighboring Er^{3+} ions becomes weaker and the quenching concentration of $^2H_{11/2}/^4S_{3/2}$ in Er^{3+} ions is enhanced. Compared to the sample without Bi^{3+} (inset of Fig. 1), the ratio of green to red emission decreases with Bi^{3+} doping (inset of Fig. 7), which implies that the cross-relaxation processes $^4F_{7/2} \rightarrow {}^4F_{9/2}$ and $^4F_{9/2} \leftarrow {}^4I_{11/2}$ are decreased by adding Bi^{3+}.

Fig. 8 shows the emission spectra of 5.0 mol% Er^{3+} and 1.5 mol% Bi^{3+} codoped Y_2O_3 and 3.0 mol% Er^{3+} doped Y_2O_3. As shown in Fig. 8, the position of emission peaks does not vary with Bi^{3+} doping. However, we observe a noticeable increase in the luminescence

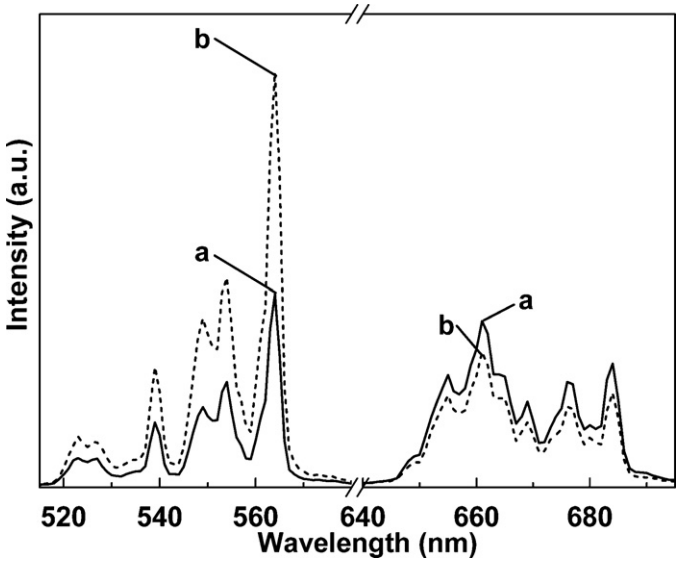

Fig. 8. Green and red upconversion emissions of (a) 3.0 mol% $Er^{3+}:Y_2O_3$ and (b) 1.5 mol% Bi^{3+}/5.0 mol% $Er^{3+}:Y_2O_3$ under 980 nm excitation and a excitation power of 200 mW.

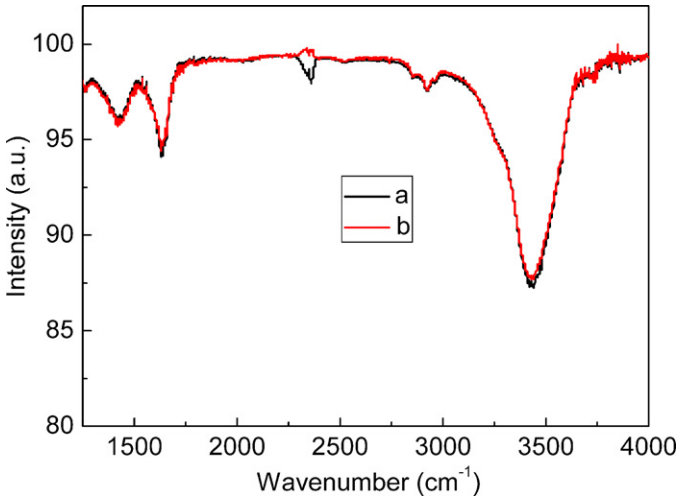

Fig. 9. FT-IR spectra of (a) 3.0 mol% $Er^{3+}:Y_2O_3$ and (b) 1.5 mol% Bi^{3+}/5.0 mol% $Er^{3+}:Y_2O_3$.

intensity of green emission, about 1.9 times, for the sample doped with Bi^{3+} compared to the undoped counterpart. Meanwhile, an obvious decrease in the red emission is observed. In order to clarify the mechanism of the enhancement of green emission, the FT-IR spectra in Y_2O_3 doped with different concentrations of Er^{3+} and Bi^{3+} are measured. It is known that CO_3^{2-} and OH^- groups with high vibrations frequencies of 1500 and 3350 cm^{-1} will increase the nonradiative relaxation rate and hence decrease upconversion efficiency [18]. As shown in Fig. 9, the intensity of the 1500 and 3350 cm^{-1} bands in the two samples are almost the same. This means that the different upconversion efficiencies do not come from CO_3^{2-} and OH^- groups. So the enhancement of green emission is caused by two reasons: one is the increase of the quenching concentration of $^2H_{11/2}/^4S_{3/2}$, which populates the $^2H_{11/2}/^4S_{3/2}$ level; the other is the modification of the crystal field around Er^{3+}, which increases the radiative transition ratio. According to our previous research, the modification of the crystal field can contribute a factor of 1.5 to the total enhancement of green emission [16]. The increased quenching concentration of $^2H_{11/2}/^4S_{3/2}$ level thus contributes a factor of about 1.3 to the total enhancement factor of 1.9.

4. Conclusions

The interaction between neighboring Er^{3+} ions is decreased after Bi^{3+} doping. As a result, the quenching concentration of $^2H_{11/2}/^4S_{3/2}$ in Er^{3+} ions increases by 2.0 mol%. Furthermore, the doping of larger radius Bi^{3+} breaks the crystal field around Er^{3+}, and then increases the radiative transition ratio of Er^{3+}. The green emission enhances 1.9 times by increasing in both quenching concentration of $^2H_{11/2}/^4S_{3/2}$ and radiative transition.

Acknowledgments

This work was supported by the National Natural Science Foundation of China (Grant Nos. 50672019 and 10804024) and the Scientific Research Foundation for the Returned Overseas Chinese Scholars, State Education Ministry. Supported by "the Fundamental Research Funds for the Central Universities" (Grant No. HIT.NSRIF.2009056).

References

[1] X.D. Qi, C.M. Liu, C.C. Kuo, J. Alloys Compd. 492 (2010) L61.
[2] B.J. Chen, E.Y.B. Pun, H. Lin, J. Alloys Compd. 479 (2009) 352.

[3] S.F. Lim, R. Riehn, W.S. Ryu, N. Khanarian, C.K. Tung, D. Tank, R.H. Austin, Nano Lett. 6 (2006) 169.
[4] A. Patra, C.S. Friend, R. Kapoor, P.N. Prasad, J. Phys. Chem. B 106 (2002) 1909.
[5] Q. Sun, X.Q. Chen, Z.K. Liu, F.P. Wang, Z.H. Jiang, C. Wang, J. Alloys Compd. 509 (2011) 5336.
[6] D. Li, B. Dong, X. Bai, Y. Wang, H.W. Song, J. Phys. Chem. C 114 (2010) 8219.
[7] R. Srinivasan, N.R. Yogamalar, J. Elanchezhiyan, R.J. Joseyphus, A.C. Bose, J. Alloys Compd. 496 (2010) 472.
[8] Y.P. Li, J.H. Zhang, X. Zhang, Y.S. Luo, S.Z. Lu, Z.D. Hao, X.J. Wang, J. Phys. Chem. C 113 (2009) 17705.
[9] X.P. Qin, G.H. Zhou, H. Yang, Y. Yang, J. Zhang, S.W. Wang, J. Alloys Compd. 493 (2010) 672.
[10] X. Wang, G.Y. Shan, K.F. Chao, Y.L. Zhang, R.L. Liu, L.Y. Feng, Q.H. Zeng, Y.J. Sun, Y.C. Liu, X.G. Kong, Mater. Chem. Phys. 99 (2006) 370.
[11] L.G. Jacobsohn, M.W. Blair, S.C. Tornga, L.O. Brown, B.L. Bennett, R.E. Muenchausen, J. Appl. Phys. 104 (2008) 124303.
[12] M.Z. Yang, Y. Sui, S.P. Wanga, X.J. Wanga, Y.Q. Sheng, Z.G. Zhang, T.Q. Lü, W.F. Liu, Chem. Phys. Lett. 492 (2010) 40.
[13] S.H. Shin, J.H. Kang, D.Y. Jeon, D.S. Zang, J. Lumin. 114 (2005) 275.
[14] C.G. Dou, Q.H. Yang, X.M. Hu, J. Xu, Opt. Commun. 281 (2008) 692.
[15] R.D. Shannon, Acta Crystallogr. A32 (1976) 751.
[16] M.Z. Yang, Y. Sui, S.P. Wang, X.J. Wang, Y. Wang, S.C. Lü, Z.G. Zhang, Z.G. Liu, T.Q. Lü, W.F. Liu, J. Alloys Compd. 509 (2011) 827.
[17] F. Vetrone, J.C. Boyer, J.A. Capobianco, J. Appl. Phys. 96 (2004) 661.
[18] H. Guo, N. Dong, M. Yin, W.P. Zhang, L.R. Lou, S.D. Xia, J. Phys. Chem. B 108 (2004) 19205.